

Measuring On-Line and Off-Line Noncontact Ultrasound Time of Flight Weld Penetration Depth

Presented is the development of a new RGLS time of flight technique for weld penetration measurements, along with other time of flight techniques

BY A. KITA AND I. C. UME

ABSTRACT. Welding is the primary technique used for joining structural components. However, weld penetration depth measurement is not done in real-time resulting in open-loop control of it. The major obstacle to on-line weld penetration depth measurement is a lack of accurate and high-resolution nondestructive and noncontact sensors that can operate in high temperatures and harsh environments typical of welding processes. The use of ultrasonic sensors to measure weld penetration depth of butt joint welds has focused on using a direct reflection of either a longitudinal or shear wave from the bottom of a weld bead.

During laser generation of ultrasound, it was observed that a Rayleigh (surface) wave was generated on the bottom of weld samples. This Rayleigh wave traveled to the bottom of the weld bead where it mode converted into a longitudinal (pressure) and shear (transverse) wave. The mode-converted longitudinal wave traveled to the bottom of the weld sample where it generated a shear (RGLS) and longitudinal (RGLL) wave reflection. Similarly, the mode converted shear wave also generated a shear (RGSS) and longitudinal (RGSL) wave reflection. The development of a new RGLS time of flight (TOF) technique for weld penetration measurements will be presented. Experimental results using the RGLS TOF technique for weld penetration depth measurement has proven to be accurate, precise, and repeatable both off-line after welding and on-line during welding. Additional RGLL, RGSL, and RGSS TOF techniques related to the RGLS TOF technique will also be presented. This new technique for measuring weld penetration depth can enable closed loop control of weld penetration depth.

A. KITA and I. C. UME (charles.ume@me.gatech.edu) are with G.W. Woodruff School of Mechanical Engineering, Georgia Institute of Technology, Atlanta, Ga.

Introduction

Welding is the primary technique used for joining structural components. Welding is practiced in almost every industry, and it is used extensively in civil construction, shipbuilding, offshore platforms, pipe laying, and boiler and nuclear plant component fabrication. Therefore, welding plays a crucial role in determining the cost and quality of finished products and structures. A large percentage of welds are formed by butt joint welding. The weld must penetrate the correct distance into the seam in butt joint welded components. The welded components must be either scrapped or rewelded when optimum penetration depth is not achieved. This reduces productivity and increases product costs. Insufficient weld penetration depth can result in in-service failures and loss of human life if left undetected.

The major obstacle to on-line weld penetration depth measurement is a lack of accurate and high-resolution nondestructive and noncontact techniques using sensors that can operate in high-temperature and harsh environments typical of welding processes. Techniques currently studied by researchers can be subdivided into four distinct categories — through-arc sensing of current and voltage; sensing the thermal distribution in and around the weld pool; weld bead measurement using machine vision; and ultrasonic sensing. Arc sensing of current and voltage can

only detect disturbances in the welding process and cannot measure weld penetration depth (Refs. 1, 2). Determination of the thermal distribution in and around the weld pool and weld bead measurement using machine vision allows for determining only the weld pool size and shape on the top surface (Refs. 3–7). Theoretically, ultrasound can be used to probe weld penetration depth. However, there is no nondestructive and noncontact ultrasound techniques available to measure weld penetration depth on-line and off-line.

Prior ultrasound research in the area of weld penetration depth measurement of butt joint welds has focused on using a direct reflection of either the longitudinal or shear ultrasonic wave from the bottom of the weld bead (Refs. 8–12). The majority of prior research used a pulsed laser to generate ultrasound and an electro-magnetic acoustic transducer (EMAT) to receive ultrasound. Laser ultrasound generation is well established and understood (Refs. 13–18). Laser phased arrays were developed to strengthen the direct reflection of the longitudinal or shear wave from the bottom of the weld bead (Refs. 19–22). Laser generation of ultrasound and EMAT reception of ultrasound are both noncontact. However, the combination of laser ultrasound generation and EMAT reception presents a problem when trying to use either a direct reflection of the longitudinal or shear wave from the bottom of the weld bead to measure weld penetration depth. Ultrasound is not efficiently received or generated at the shallow angles required for a direct reflection of the longitudinal or shear wave from the bottom of the weld bead.

A simple experiment was carried out to see if a shear wave reflected from the bottom of a weld bead can be observed using laser ultrasound generation and EMAT reception when the generation and reception locations are 0.16 m apart as shown in Fig. 1. A Laser Photonics Nd:Yag with a 12

KEYWORDS

Rayleigh Wave
Nondestructive Testing
Penetration Depth
Ultrasound
Time of Flight (TOF)
Electro-Magnetic Acoustic
Transducer (EMAT)

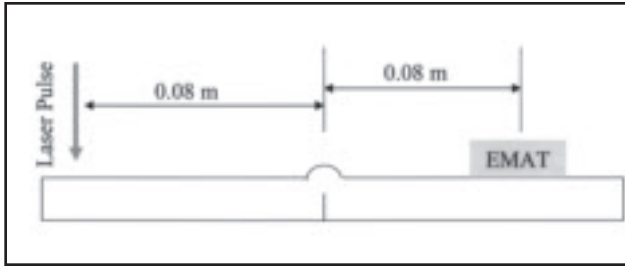


Fig. 1 — Experimental setup 1 to measure shear wave.

ns pulse time, 650 mJ per pulse, and 1064 nm wavelength was used to generate ultrasound.

All experiments presented in this article use ablation as the laser ultrasound generation method. The EMAT is a custom shear wave EMAT (LURL EMAT) developed at Georgia Tech. The signal from the EMAT was filtered using a Khron-hite filter to limit bandwidth to 5 MHz. A Gage 6012 PCI data acquisition card was used to digitize the signal from the EMAT at 30 Msamples/s. The prewelded test specimen of 1018 mild steel has a weld penetration depth of 3 mm. The specimen was welded with a Miller Pulstar 450 GMAW machine. The weld gun is moved by a General Electric P-50 process robot. All welding is automated. Pro-Tec 3, a 75/25% ratio of argon and CO₂, is used as the shielding gas. Welding wire is 0.035-in.-diameter carbon steel with a specification of AWS A5.18 class E70S-3. Filler metal is deposited into the weld joint using the globular transfer method. The voltage used was 25 V with a fixed 0.5 in. gun to weld joint height. Any oxidation on the weld joint surface is removed with a grinder prior to welding.

The received signal is shown in Fig. 2, and the theoretical shear wave time of flight (TOF) for the shear wave reflected from the bottom of the weld bead is labeled. The shear wave reflected from the bottom of the weld bead was very weak and difficult to consistently detect. There is another stronger wave preceding it. This wave is not the longitudinal wave reflected from the bottom of the weld bead. The TOF of the wave did not match any TOF of previously researched waves. Therefore, the wave will be referred to as the unknown wave. As it turns out, determining the path this unknown wave travels is the key to consistent weld penetration depth measurement.

Discovery of the RGLS Mode Converted Wave

Two experimental setups were used to determine the unknown wave path. Experimental setup 2,

shown in Fig. 3, is used to determine the unknown wave's path on the generation side of the weld bead. In experimental setup 2, the distance between the ultrasound generation point and weld bead was varied. The equipment and weld sample used are the same as the first experiment. Experimental setup 3, shown in Fig. 4, is used to determine the unknown wave's path on the reception side of the weld bead. In experimental setup 2, the distance between the LURL EMAT and weld bead was varied. The equipment and weld sample used are the same as the first experiment.

Experimental results are shown in Figs. 5 and 6 for experimental setup 2 and 3, respectively. Blue circles indicate arrival times for the unknown wave for different variable distances. Red lines are linear fits of the data where the slope indicates speed in m/s. The dependent variable is shown on the horizontal axis, and the independent variable is on the vertical axis. This was done so that the slope of the linear fit is in m/s.

These speeds are then compared to known speeds for longitudinal, shear, and Rayleigh ultrasonic waves in steel. The known speed for longitudinal, shear, and Rayleigh ultrasonic waves in steel are 5960, 3240, and 3000 m/s, respectively (Ref. 8). For experimental setup 2, the linear fit indicates a speed of approximately 3004 m/s. This indicates that the unknown wave is traveling as a Rayleigh wave between the generation point and weld. For experimental setup 3, the linear fit indicates a speed of approximately 5790 m/s. This indicates that the unknown wave has a longitudinal component between the weld and reception point. The unknown wave must be traveling as a longitudinal to shear (LS) mode-converted wave between the weld and reception point since the LURL EMAT cannot detect longitudinal waves.

A slot was cut into the top of the sample between the generation point and weld to determine if the Rayleigh component of the unknown wave was traveling on the

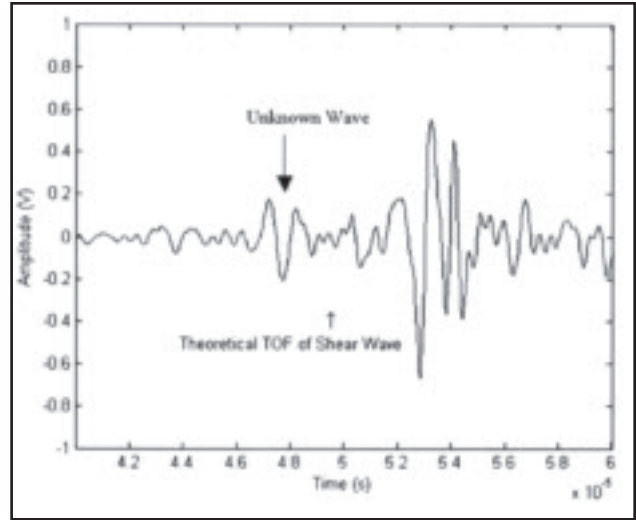


Fig. 2 — Received EMAT signal from experimental setup 1.

top or bottom surface. The received waveform is shown in Fig. 7. The experimental results show that the unknown wave still propagates though while the Rayleigh wave on the top surface is reflected back toward the generation point by the slot. Therefore, the unknown wave is traveling on the bottom surface as a Rayleigh wave.

If the Rayleigh wave generated on the top surface had traveled around the sample to the bottom, the slope seen for experimental setup 2 would be -3004 ms. The Rayleigh wave on the bottom surface must have been created from a bulk wave. Careful thought about the nature of a Rayleigh wave and physics behind Snell's law can lead to an answer. Rayleigh waves are a combination of shear and longitudinal waves. Snell's law enforces the relationship between wavelength and wave speed. A laser pulse on the surface generates both shear and longitudinal waves as a hemispherical wave front within the bulk of the material. There is an angle, θ_{GL} , within the generated longitudinal hemispherical wave front where the horizontal component of the longitudinal wavelength, λ_L , matches the Rayleigh wavelength, λ_R . Similarly, there is an angle θ_{GS} within the generated shear hemispherical wave front where the horizontal component of the shear wavelength, λ_S , matches the Rayleigh wavelength, λ_R . These relationships are shown in Fig. 8.

Equations for θ_{GL} and θ_{GS} are given in Equations 1 and 2, respectively.

$$\theta_{GL} = a \sin \left(\frac{C_R}{C_L} \right) \quad (1)$$

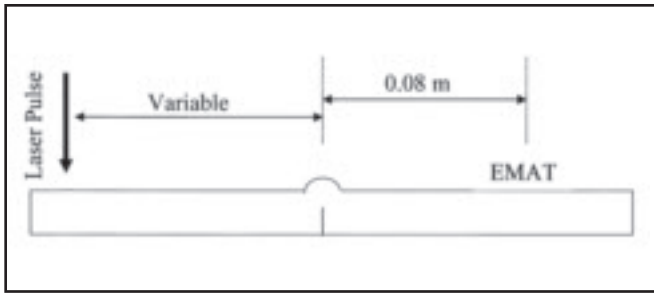


Fig. 3 — Experimental setup 2.

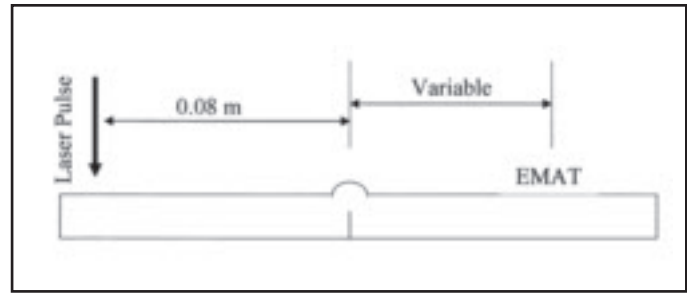


Fig. 4 — Experimental setup 3.

Table 1 — RGLS Method Weld Penetration Depth Measurement Results from Day 1

Sample Number	Actual Penetration Depth (mm)	RGLS TOF Penetration Depth (mm)	Difference (mm)	Absolute Percent Error
A1	3.06	2.98	8.53E-02	2.79
A2	2.76	2.70	6.05E-02	0.05
A3	3.02	3.07	-4.89E-02	-1.62
A4	3.86	3.82	3.40E-02	0.88
A5	3.19	3.17	2.40E-02	0.75
A6	4.81	4.77	3.72E-02	0.77
A7	4.09	4.01	8.10E-02	1.98
A8	2.70	2.79	-9.00E-02	-3.33
A9	4.72	4.68	4.50E-02	0.95
A10	4.38	4.39	-1.20E-02	-0.27
A11	3.81	3.78	3.30E-02	0.87
A12	3.37	3.35	1.82E-02	0.54
A13	4.51	4.58	-7.00E-02	-1.55
A14	4.03	4.01	1.40E-02	0.35
A15	5.35	5.34	1.00E-02	0.19

- Average absolute percent error: 1.27%
- Minimum percent error: 0.19%
- Maximum percent error: 3.33%
- Standard deviation of differences: 5.11×10^{-2} mm

$$\theta_{GS} = a \sin\left(\frac{C_R}{C_S}\right) \quad (2)$$

Assume that a Rayleigh wave is generated between where the longitudinal wave and shear wave strike the bottom surface. Since the thickness, T , is known, the location on the bottom surface where the Rayleigh wave is generated can be calculated using Equation 3 where $\theta_{RG} = (\theta_{GL} + \theta_{GS})/2$. The time between ultrasound generation on the top surface and Rayleigh wave generation on the bottom surface, t_{RG} , depends on when the shear wave front reaches the generation point and can be calculated using Equation 4.

$$D_{RG} = T \cdot \tan(\theta_{RG}) \quad (3)$$

$$t_{RG} = \frac{T}{C_s \cos(\theta_{RG})} \quad (4)$$

There are two conditions that must be met for a Rayleigh wave to be generated on the bottom surface from bulk waves. Shear and longitudinal wave fronts must be created simultaneously at the ultrasound generation point. A portion of the shear and longitudinal wave fronts must be at the correct angles, θ_{GL} and θ_{GS} . Laser ultrasound generation by ablation will always ensure these two conditions are met.

The complete path for the unknown wave is shown in Fig. 9. The unknown wave will be referred to as the RGLS mode converted wave. The Rayleigh wave generated on the bottom surface travels toward the weld joint. At the weld joint, the Rayleigh wave propagates to the bottom of the weld bead. At the bottom of the weld bead, part of the Rayleigh wave energy is converted into shear and longitudinal waves (Ref. 23). These shear and lon-

gitudinal waves have spherical wave fronts propagating away from the bottom of the weld bead. A portion of the spherical longitudinal wave front will strike the bottom surface at the correct angle to generate a shear wave to the receiver.

Theoretical TOF for the RGLS mode converted wave can be calculated by using the following equations:

$$RGLS_{TOF} = t_{RG} + \frac{(D_{GW} + T - PD - D_{RG})}{C_R} + \frac{T - PD}{C_L \cos(\theta_{L1})} + \frac{T}{C_S \cos(\theta_{S1})} \quad (5)$$

where:

C_R , C_S , C_L : Rayleigh, shear, and longitudinal wave speeds

t_{RG} : Time for RG wave generation

D_{RG} : Horizontal distance between ultrasound generation point and RG wave generation point

D_{GW} : Distance between ultrasound generation point and weld joint

D_{WR} : Distance between weld joint and ultrasound sensor

T : Sample thickness or distance between opposite surfaces

PD : Penetration depth of weld

θ_{S1} : Reflection angle of shear wave from bottom surface

θ_{L1} : Reflection angle of longitudinal wave from bottom surface

The following two equations must be iterated to find θ_{S1} and θ_{L1} .

$$\frac{\sin(\theta_{S1})}{C_S} = \frac{\sin(\theta_{L1})}{C_L} \quad (6)$$

$$D_{WR} = T \cdot \tan(\theta_{S1}) + (T - PD) \tan(\theta_{L1}) \quad (7)$$

Comparison of the theoretical RGLS TOF and experimental data is shown in Fig. 10 and shows good agreement.

The RGLS mode converted wave can

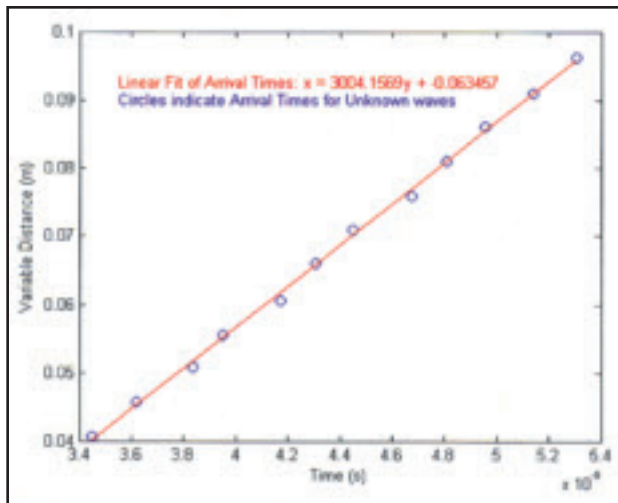


Fig. 5 — Results for experimental setup 2.

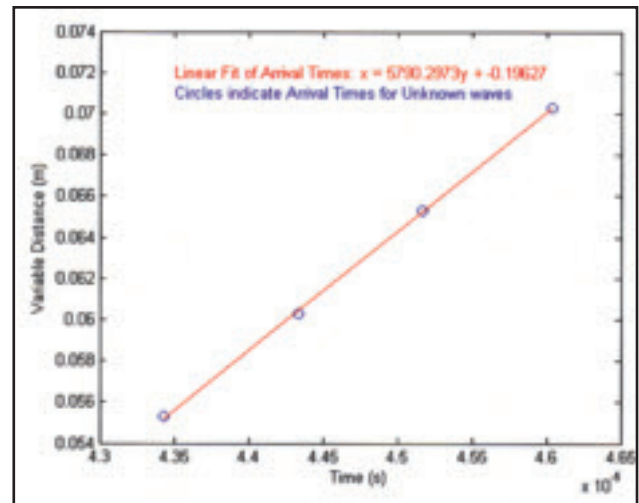


Fig. 6 — Results for experimental setup 3.

Table 2 — RGLS Method Weld Penetration Depth Measurement Results from Day 2

Sample Number	Actual Penetration Depth (mm)	RGLS TOF Penetration Depth (mm)	Difference (mm)	Absolute Percent Error
B1	3.10	3.17	-6.30E-02	2.03
B2	4.98	4.96	1.71E-02	0.34
B3	2.13	2.14	-6.00E-03	0.28
B4	4.99	4.96	3.20E-02	0.64
B5	5.01	5.05	-4.20E-02	0.84
B6	2.15	2.14	1.50E-02	0.70
B7	5.00	4.96	4.10E-02	0.82
B8	3.96	3.92	4.30E-02	1.09
B9	2.10	2.14	-3.69E-02	1.76
B10	3.72	3.82	-1.04E-01	2.79

- Average absolute percent error: 1.13%
- Minimum percent error: 0.28%
- Maximum percent error: 2.79%
- Standard deviation of differences: 4.94×10^{-2} mm

Table 3 — RGLS Method Weld Penetration Depth Measurement Results from Day 3

Sample Number	Actual Penetration Depth (mm)	RGLS TOF Penetration Depth (mm)	Difference (mm)	Absolute Percent Error
C1	2.50	2.51	-1.40E-02	0.56
C2	3.70	3.68	2.00E-02	0.54
C3	4.26	4.25	6.00E-03	0.14
C4	3.57	3.50	7.00E-02	1.96
C5	4.36	4.34	1.50E-02	0.34
C6	5.34	5.40	-6.10E-02	1.14
C7	4.08	4.06	1.60E-02	0.39
C8	4.42	4.44	-2.30E-02	0.52
C9	2.95	2.93	1.30E-02	0.44
C10	3.60	3.59	9.00E-03	0.25

- Average absolute percent error: 0.64%
- Minimum percent error: 0.14%
- Maximum percent error: 1.96%
- Standard deviation of differences: 3.51×10^{-2} mm

RGLS mode converted wave has a much higher amplitude and is easier to detect. The high signal strength of the acquired RGLS mode converted wave enables the laser ultrasound generation point and EMAT to be placed farther away from the weld bead and welding torch thus reduces the chances of damage from high heat or weld spatter.

RGLS TOF Technique of Measuring Weld Penetration Depth Off-Line After Welding

The RGLS mode converted wave TOF technique of measuring weld penetration depth off-line after welding uses the same experimental setup as experimental setup 1. A prewelded sample is placed into the experimental setup. Welding gun speed and wire feed rate were varied to achieve different weld penetration depths. Eight signals are digitized and averaged. The experimental RGLS mode converted wave TOF is measured by finding the maximum absolute amplitude before the Rayleigh wave in the averaged signal. Equations 5 through 7 are iterated by varying a guess of penetration depth until the theoretical RGLS mode converted wave TOF matched the experimental RGLS mode converted wave TOF. Iteration was done using the bisection method. The final guessed penetration depth is the measured penetration depth and is compared to actual penetration depth. The actual penetration depth was measured by taking a picture of the weld cross section using an optical scanner at 2400×2400 pixels per in. resolution (1.06×10^{-2} mm \times 1.06×10^{-2} mm resolution).

Thirty-five prewelded samples were measured over three days. Fifteen prewelded samples were measured during

be used to measure weld penetration depth since it travels from the bottom of the weld sample to the bottom of the weld bead. Since the RGLS mode converted wave travels from the laser ultrasound

generation point to the weld bead mainly as a Rayleigh wave, the RGLS mode converted wave is attenuated less than the shear or longitudinal wave reflected from the bottom of a weld bead. Therefore, the

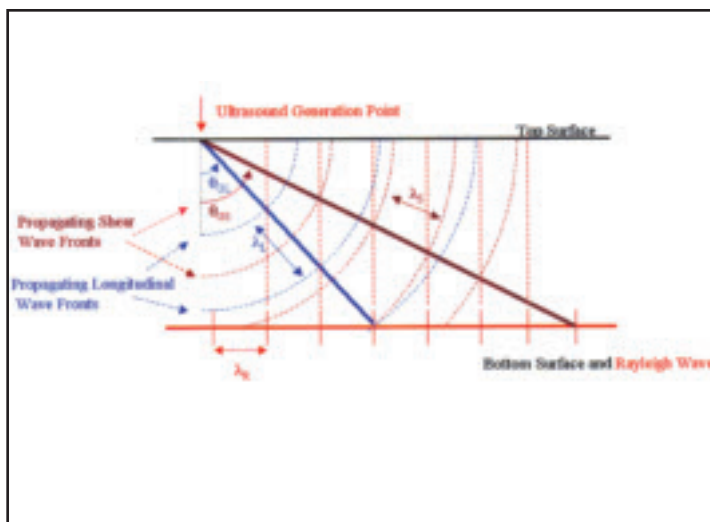
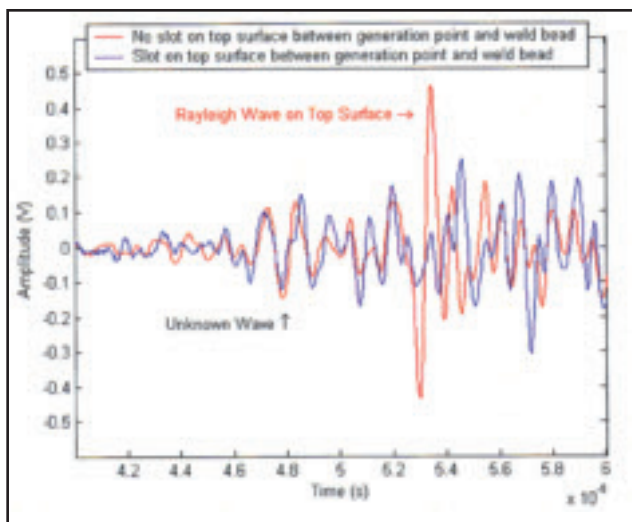


Fig. 7 — Unknown wave with and without slot between generation point and weld bead.

Fig. 8 — Determining λ_L and λ_S for Rayleigh wave generation on bottom surface.

the first day. Ten prewelded samples were measured during each of the remaining two days. The prewelded samples were measured in this manner to investigate repeatability of the RGLS TOF method. The results from each individual day are listed in Tables 1 to 3. The average, maximum, and minimum absolute percent error are given for each day. The standard deviation of the differences between measured and actual weld penetration depth is also listed.

Low percent errors show accuracy of the RGLS TOF method of finding weld penetration depth. Low standard deviation of the differences between measured and actual penetration depth show precision of the RGLS TOF method of finding weld penetration depth.

In order to demonstrate repeatability of the RGLS TOF method, measurement results for all three days were combined and are shown in Fig. 11. The combined results are plotted with the actual versus measured penetration depth. The slope of a linear fit to the data is 0.9963 and the R-squared value is 0.9973. Both the slope and R-squared value indicates a very good correlation between the actual and measured weld penetration depth. The average absolute percent error was 1.05% for the combined results. The minimum percent error was 0.14%. The maximum percent error was 3.33%. The standard deviation of differences between measured and actual penetration depth is 4.62×10^{-2} mm.

The standard deviation of the differences of the overall compared to the standard deviation of the differences for each day is within an order of magnitude. This shows repeatability of the RGLS TOF

Table 4 — Results for RGSS TOF Technique

Sample Number	Actual Penetration Depth (mm)	RGLS TOF Penetration Depth (mm)	Difference (mm)	Absolute Percent Error
D1	4.36	4.42	-6.41E-02	1.47
D2	3.57	3.51	6.10E-02	1.71
D3	4.08	3.97	1.13E-01	2.77
D4	4.42	4.41	7.96E-03	0.18
D5	3.60	3.66	-5.80E-02	1.61

- Average absolute percent error: 1.55%
- Minimum percent error: 0.18%
- Maximum percent error: 2.77%
- Standard deviation of differences: 7.69×10^{-2} mm

Table 5 — Results for RGLS TOF Technique

Sample Number	Actual Penetration Depth (mm)	RGLS TOF Penetration Depth (mm)	Difference (mm)	Absolute Percent Error
E1	2.50	2.50	1.00E-03	0.04
E2	3.70	3.72	-1.89E-02	0.51
E3	4.26	4.23	2.90E-02	0.68
E4	5.34	5.30	4.49E-02	0.84
E5	2.95	2.98	-2.71E-02	0.92

- Average absolute percent error: 0.60%
- Minimum percent error: 0.04%
- Maximum percent error: 0.92%
- Standard deviation of differences: 3.08×10^{-2} mm

method of finding weld penetration depth. These experiments demonstrate the accuracy, precision, and reliability of the RGLS TOF method for weld penetration depth measurement off-line after welding. This is also the first method to measure weld penetration depth accurately using noncontact ultrasound generation and reception off-line after welding. However, the real goal of this overall research thrust is to measure weld penetration depth on-

line during welding. High-temperature gradients may affect the measurement of weld penetration depth.

RGLS TOF Technique of Measuring Weld Penetration Depth On-Line During Welding

An experiment was done to see if high-temperature gradients affect the mea-

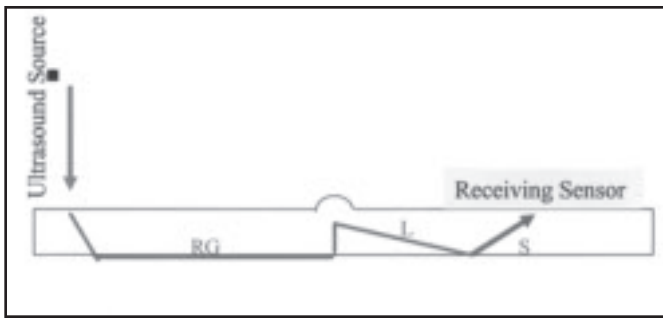


Fig. 9 — Path of RGLS mode converted wave.

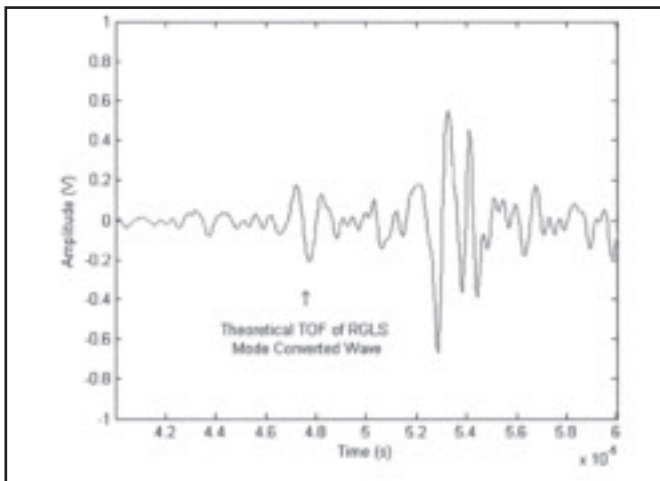


Fig. 10 — Comparison of theoretical RGLS TOF and experimental data.

sured RGLS wave during welding. The experimental setup is shown in Fig. 12. LURL EMAT was used as the receiving sensor and a Laser Photonics ND:YAG laser was used for generating ultrasound. The LURL EMAT and laser pulse locations are stationary. The welding torch passes between the LURL EMAT and laser pulse locations. The same welding setup as in experimental setup 1 was used.

starting weld penetration depth measurement is lower because ultrasound travels slower in high temperatures. The RGLS TOF is larger since the ultrasound travels slower. A larger RGLS TOF will result in the lower penetration depth measurement.

In Fig. 14, the welding gun speed was 0.375 in./s and the wire feed rate was 400 in./min. These parameters produced a

shallower weld than before. The RGLS TOF method of weld penetration depth measurement still converged to the actual weld penetration depth when the weld cooled sufficiently.

Each combination of wire feed rate and welding gun speed results in a different amount of time for the weld to fully solidify and cool. The ultrasound generation point and EMAT must be placed behind the welding gun in order to allow the weld to fully solidify and cool before measuring the weld penetration depth. A look-up table of distance between welding gun and weld penetration depth measurement system versus welding parameters can be created by further experimentation. For example, in Fig. 15, three trial welds are shown for 0.5 in./s gun speed and 500 in./min wire feed rate. All weld penetration depth measurements are within 0.1 mm of the actual penetration depth 13.5 s after the welding gun passes the ultrasound generation point and EMAT. The ultrasound generation point and EMAT must be placed 6.75 inches (13.5 s * 0.5 in./s) behind the welding gun.

In Fig. 13, the welding gun speed was 0.5 in./s and the wire feed rate was 500 in./min. The RGLS wave first starts to be received around 0.5 seconds after the gun passes. From 0 to 0.5 seconds, the weld is still molten. The Rayleigh wave generated on the bottom surface cannot generate a longitudinal wave at the bottom of the molten weld bead. Therefore, the RGLS wave cannot form when the weld bead is still molten. When the RGLS wave is received, the measured weld penetration starts lower than the actual penetration depth and approaches the actual weld penetration depth around 9 s after the welding gun passes. The

shallow weld than before. The RGLS TOF method of weld penetration depth measurement still converged to the actual weld penetration depth when the weld cooled sufficiently.

Each combination of wire feed rate and welding gun speed results in a different amount of time for the weld to fully solidify and cool. The ultrasound generation point and EMAT must be placed behind the welding gun in order to allow the weld to fully solidify and cool before measuring the weld penetration depth. A look-up table of distance between welding gun and weld penetration depth measurement system versus welding parameters can be created by further experimentation. For example, in Fig. 15, three trial welds are shown for 0.5 in./s gun speed and 500 in./min wire feed rate. All weld penetration depth measurements are within 0.1 mm of the actual penetration depth 13.5 s after the welding gun passes the ultrasound generation point and EMAT. The ultrasound generation point and EMAT must be placed 6.75 inches (13.5 s * 0.5 in./s) behind the welding gun.

Alternatives to RGLS TOF Technique of Measuring Weld Penetration Depth

The Rayleigh wave traveling on the bottom surface can generate waves other than the RGLS mode converted wave when it reaches the bottom of the weld bead. These include the RGSS, RGSL, and RGLL mode converted waves and are shown in Figs. 16 through 18.

Theoretical TOF for the RGSS, RGSL, and RGLL waves are shown in Equations 8–10. Equations 11 and 12 must be solved iteratively to find θ_{S1} and θ_{L1} for the RGSL mode converted wave.

$$RGLL_{TOF} = t_{RG} + \frac{(D_{GW} + T - PD - D_{RG})}{C_R} + \frac{\sqrt{(2 \cdot T - PD)^2 + D_{WR}^2}}{C_L} \quad (8)$$

$$RGSL_{TOF} = t_{RG} + \frac{(D_{GW} + T - PD - D_{RG})}{C_R} + \frac{T}{C_L \cos(\theta_{L1})} + \frac{T - PD}{C_S \cos(\theta_{S1})} \quad (9)$$

Table 6 — Results for RGSL TOF Technique

Sample Number	Actual Penetration Depth (mm)	RGLS TOF Penetration Depth (mm)	Difference (mm)	Absolute Percent Error
E1	2.50	2.47	3.20E-02	1.28
E2	3.70	3.66	3.59E-02	0.97
E3	4.26	4.19	7.50E-02	1.76
E4	5.34	5.30	3.52E-02	0.66
E5	2.95	2.99	-3.89E-02	1.32

- Average absolute percent error: 1.20%
- Minimum percent error: 0.66%
- Maximum percent error: 1.76%
- Standard deviation of differences : 4.13×10^{-2} mm

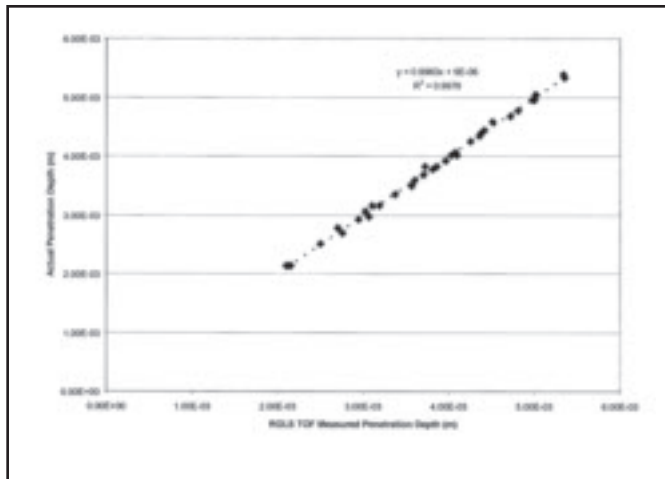


Fig. 11 — Combined results.

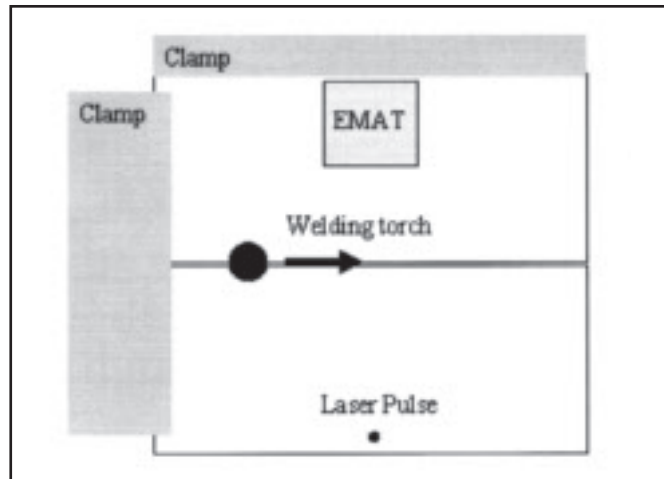


Fig. 12 — Top view of experimental setup to determine if high-temperature gradients affect measured weld penetration depth during welding.

$$RGSS_{TOF} = t_{RG} + \frac{(D_{GW} + T - PD - D_{RG})}{C_R} + \frac{\sqrt{(2 \cdot T - PD)^2 + D_{WR}^2}}{C_S} \quad (10)$$

$$\frac{\sin(\theta_{S1})}{C_S} = \frac{\sin(\theta_{L1})}{C_L} \quad (11)$$

$$D_{WR} = (T - PD) \cdot \tan(\theta_{S1}) + T \cdot \tan(\theta_{L1}) \quad (12)$$

The RGSS, RGSL, and RGLL mode converted waves travel from the bottom of the weld sample to the bottom of the weld bead and can be used to measure weld penetration depth. These waves were used to measure five samples each in experiments similar to the RGLS mode converted wave off-line weld penetration depth measurement experiment. A Valpey-Fisher VP-1093 longitudinal wave PZT was used instead of the EMAT when the RGSL and RGLL mode converted waves were used. The results are shown in Tables 4 to 6.

It is apparent that the RGSS, RGSL, and RGLL TOF techniques have a similar accuracy as the RGLS TOF technique. The selection of technique depends on the type of ultrasound sensor employed. The RGSL and RGLL TOF techniques can be

used when the ultrasound sensor can acquire longitudinal waves. The RGLS and RGSS TOF techniques can be used when the ultrasound sensor can acquire shear waves. The RGSS wave is the slowest. The RGSS wave may be masked by the Rayleigh wave generated on the top surface when the distance between ultrasound generation and reception points is larger than the thickness of the butt joint welded samples. The RGLL mode converted wave is the fastest. The RGLL wave may be masked by the Rayleigh wave generated on the top surface when the distance between ultrasound generation and reception points is smaller than the thickness of the butt joint welded samples.

Conclusion

Experiments used to determine the RGLS mode converted wave path have been presented. The RGLS mode converted wave path is dependent on a unique method of Rayleigh wave generation using bulk waves. Theoretical reasons why this unique Rayleigh wave generation method functions were given. The theo-

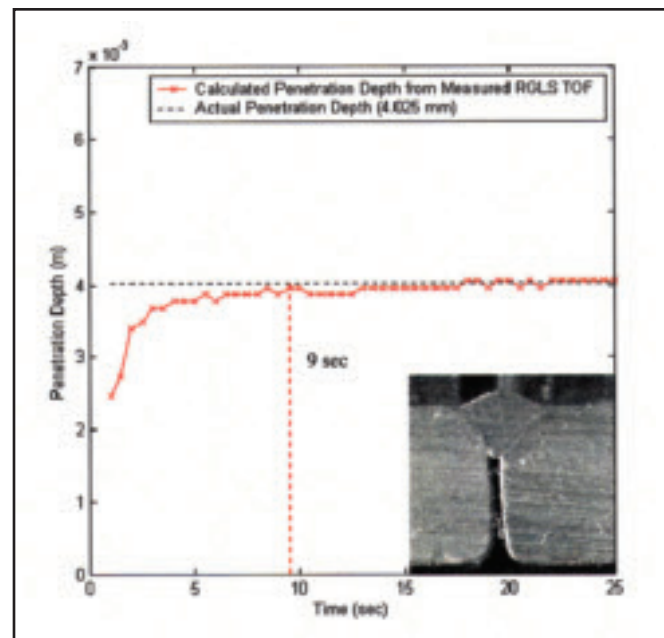


Fig. 13 — Measured penetration depth vs. time; 0.5 in./s welding gun speed, 500 in./min wire feed rate.

retical TOF equations for the RGLS mode converted wave were derived. The RGLS mode converted wave path travels from the bottom of a weld sample to the bottom of the weld bead. Therefore, the RGLS mode converted wave's TOF depends on the weld penetration depth.

Experimental results using the RGLS TOF technique for weld penetration depth measurement, laser ultrasound generation, and EMAT ultrasound reception have proven to be accurate, precise, and repeatable both off-line after welding and on-line during welding. The experimental setup in this paper has a 0.1-mm resolu-

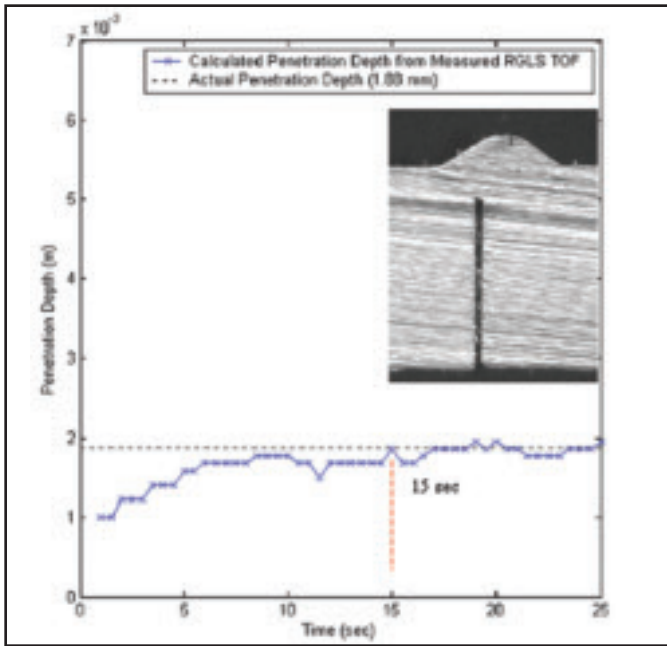


Fig. 14 — Measured penetration depth vs. time; 0.375 in./s welding gun speed, 400 in./min wire feed rate.

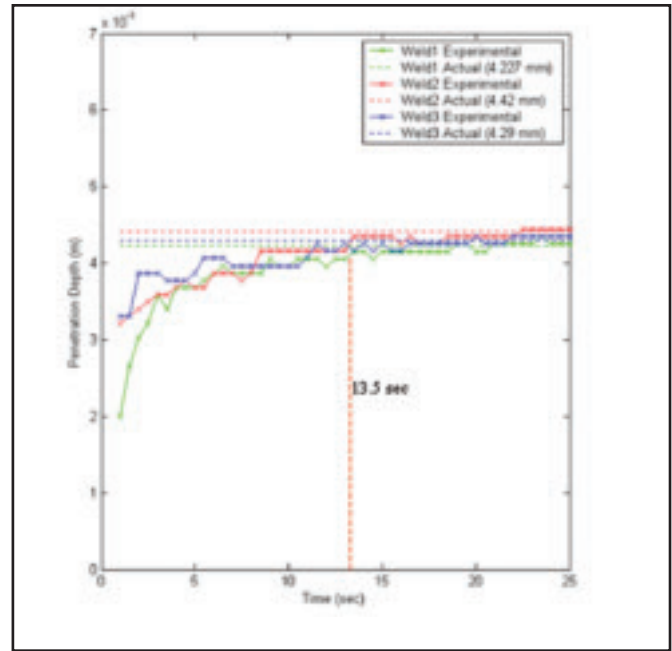


Fig. 15 — Measured penetration depth vs. time for three samples; 0.5 in./s gun speed, 500 in./min wire feed rate.

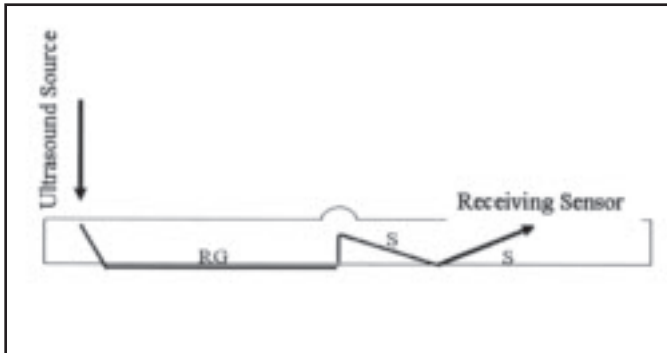


Fig. 16 — Path of RGSS mode converted wave.

tion. The resolution can be improved by using a faster data acquisition card. The laser ultrasound generation and reception points must be placed some distance behind the welding gun in order to give the weld a chance to solidify before measuring weld penetration depth.

The RGLL, RGSL, and RGSS mode converted waves related to RGLS mode converted waves were also presented and theoretical TOF equations were derived. Experimental results using the RGLL, RGSL, and RGSS TOF techniques for measuring weld penetration depth off-line show similar accuracy as the RGLS TOF measurements.

These new techniques for measuring weld penetration depth can be incorporated into a robotic welding machine. This will enable closed loop control of weld

penetration depth and quality. Costs associated with scrapping and reworking bad welds will be lowered by using closed loop control. Improved efficiency and quality from robotic welding machines will enable them to be used for critical welding tasks usually done by human welders. This will reduce workplace injuries and accidents.

References

1. Lin, R., and Fischer, G. 1995. An online arc welding quality monitor and process control system. *International IEEE/IAS Conference on Industrial Automation and Control: Emerging Technologies*, pp. 22–29.
2. Barborak, D., Conrardy, C., Madigan, B., and Paskell, T. 1999. Through-arc process monitoring techniques for control of automated gas metal arc welding. *Proceeding of the 1999 IEEE International Conference on Robotics & Automation*, pp. 3053–3058.
3. Nagarajan, S., Banerjee, P., Chen, W., and Chin, B. A. 1992. Control of the welding process using infrared sensors. *IEEE Transactions on Robotics and Automation*, Vol. 8, No. 1, pp. 86–93.
4. Santos, T. O., Caetano, R. B., Lemos, J. M., and Coito, F. J. 2000. Multipredictive adap-

tive control of arc welding trailing centerline temperature. *IEEE Transactions on Control Systems Technology*, Vol. 8, No. 1, pp. 159–169.

5. Brzakovic, D., and Khani, D. T. 1991. Weld pool edge detection for automated control of welding. *IEEE Transactions on Robotics and Automation*, Vol. 7, No. 3, pp. 397–403.

6. Kaneko, Y., Yamane, S., Kugal, K., and Ohshima, K. 1994. Neural control of weld pool in the robotic welding. *Conference Record of the Industry Applications Society Annual Meeting*, Vol. 3, pp. 1914–1919.

7. Peng, J., Chen, Q., Lu, J., Jin, J., and Van Luttervelt, C. A. 1998. Real time optimizations of robotic arc welding based on machine vision and neural networks. *Proceedings of the 24th Annual Conference of the IEEE Industrial Electronics Society*, Vol. 3, pp. 1279–1280.

8. Graham, G., Ume, C., and Hopko, S. 2000. Laser ultrasonic sensing of penetration depth in robotic welding: simulated liquid welds. *ASME Journal of Manufacturing Science and Engineering* 122(1): 70–75.

9. Graham, G. M., and Ume, I. C. 1997. Automated system for laser ultrasonic sensing of weld penetration. *Mechatronics* 7(8): 711–721.

10. Graham, G. M., Sanderson, T. M., and Ume, I. C. 1995. Intelligent welding with laser ultrasonic sensing. *Proceedings of 1st World Congress on Intelligent Manufacturing Processes*, pp. 1043–53.

11. Miller, M., Mi, B., Kita, A., and Ume, C. 2002. Development of automated real-time data acquisition system for robotic weld quality monitoring. *Mechatronics* 12(9-10): 1259–69.

12. Mi, B., and Ume, I. C. 2004. 3-D ray tracing of laser ultrasound for weld penetration sensing. *Journal of Acoustic Society of America* 115(4): 1565–1572.

13. Scruby, C. B., and Drain, L. E. 1990. *Laser ultrasonics: Techniques and applications*. Bristol, UK, Adam Higler.

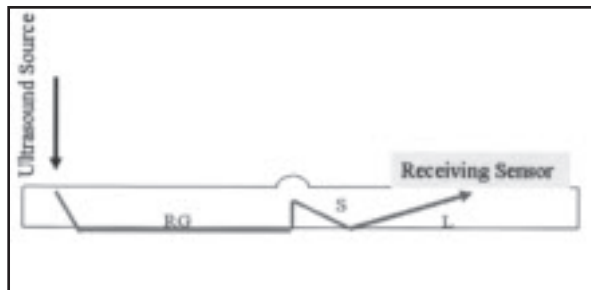


Fig. 17 — Path of RGSL mode converted wave.

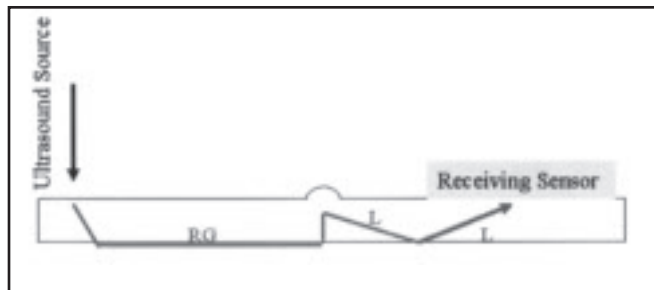


Fig. 18 — Path of RGLL mode converted wave.

14. Rose, L. R. F. 1984. Point-source representation for laser-generated ultrasound. *Journal of Acoustics Society of America* 75(3): 723–732.

15. Hutchins, D. A., Dewhurst, R. J., and Palmer, S. B. 1981. Directivity patterns of laser-generated ultrasound in aluminum. *Journal of Acoustical Society of America* 70(5): 1362–1369.

16. Umeagukwu, C., DeRidder, N., Yang, J., and Jarzynski, J. 1991. Study of the directivity patterns of laser optical fiber generated ultrasound. *121st Meeting of the JASA*, Vol. 89, No. 4, Pt. 2.

17. Sanderson, T., Ume, C., and Jarzynski, J. 1998. Longitudinal wave generation in laser ultrasound. *Ultrasonics* 35: 553–561.

18. Mi, B., and Ume, I. C. 2002. Parametric studies of laser generated ultrasound signals in ablative regime: Time and frequency domains. *Journal of Nondestructive Evaluation* 21(1): 23–33.

19. Hopko, S., and Ume, C. 1999. Laser generated ultrasound by material ablation with fiber optic delivery. *Ultrasonics* 37(1): 1–7.

20. Yang, J., DeRidder, N., Ume, C., and Jarzynski, J. 1993. Non-contact optical fiber phased array generation of ultrasound for non-destructive evolution of materials and processes. *Ultrasonics* 31(6): 387–394.

21. Murray, T. W., Marincek, M., and Wagner, J. W. 1993. Narrow-band and directed ultrasound generated by laser arrays. *Proceedings of Ultrasonics Symposium*, Vol. 1, pp. 626–639.

22. Vogel, J. A., Bruinsma, J. A., and Berkhout, A. J. 1987. Beam steering of laser generated ultrasound. *Proceedings of Ultrasonics International*, pp. 141–152.

23. Cooper, J. A., Crosbie, R. A., Dewhurst, R. J., McKie, A. D. W., and Palmer, S. B. 1986. Surface acoustic wave interactions with cracks and slots: A noncontacting study using lasers. *IEEE Transactions on Ultrasonics, Ferroelectrics, and Frequency Control*, Vol. UFFC-33, No. 5, pp. 462–470.

24. Cooper, J. A., Crosbie, R. A., Dewhurst, R. J., McKie, A. D. W., and Palmer, S. B. 1986. Surface acoustic wave interactions with cracks and slots: A noncontacting study using lasers. *IEEE Transactions on Ultrasonics, Ferroelectrics, and Frequency Control*, Vol. UFFC-33, No. 5, pp. 462–470.

CAN WE TALK?

The *Welding Journal* staff encourages an exchange of ideas with you, our readers. If you'd like to ask a question, share an idea or voice an opinion, you can call, write, e-mail or fax. Staff e-mail addresses are listed below, along with a guide to help you interact with the right person.

Publisher/Editor

Andrew Cullison
cullison@aws.org, Extension 249
 Article Submissions

Senior Editor

Mary Ruth Johnsen
mjohnsen@aws.org, Extension 238
 Feature Articles

Associate Editor

Howard Woodward
woodward@aws.org, Extension 244
 Society News
 Personnel

Assistant Editor

Kristin Campbell
kcampbell@aws.org, Extension 257
 New Products
 News of the Industry

Managing Editor

Zaida Chavez
zaida@aws.org, Extension 265
 Design and Production

Advertising Sales Director

Rob Saltzstein
salty@aws.org, Extension 243
 Advertising Sales

Advertising Sales & Promotion Coordinator

Lea Garrigan Badwy
garrigan@aws.org, Extension 220
 Production and Promotion

Advertising Production Manager

Frank Wilson
fwilson@aws.org, Extension 465
 Advertising Production

Peer Review Coordinator

Erin Adams
eadams@aws.org, Extension 275
 Peer Review of Research Papers

Welding Journal Dept.
 550 N.W. LeJeune Rd.
 Miami, FL 33126
 (800) 443-9353
 FAX (305) 443-7404